FULL TITLE
*ASP Conference Series, Vol. **VOLUME**, © **YEAR OF PUBLICATION***
NAMES OF EDITORS

Submillimeter ($\lambda < 1\,$mm) Continuum Imaging at CSO: A Retrospective

C. Darren Dowell

Jet Propulsion Laboratory, California Institute of Technology; cdd@submm.caltech.edu

Abstract. This contribution is submitted on behalf of all students, postdocs, and staff inspired and supported by Tom Phillips to build an instrument and then wait for low precipitable water vapor. Over the 20+ years of its existence, the Caltech Submillimeter Observatory (CSO) has seen a succession of ever more powerful detectors to measure continuum emission in the shortest submillimeter bands available from Mauna Kea. These instruments have been trained on the nearest solar systems, the most distant galaxies, and objects in between. I show several images collected over the 5+ year history of the SHARC II camera and anecdotal comparison with past work.

1 $\lambda < 1$ mm Continuum Detectors at CSO

A distinctive attribute of the CSO has been its support of new technologies and instruments through on-site mechanical and software assistance and the generous allocation of engineering, commissioning, and research observing time. The submillimeter continuum detectors are no exception (Figure 1).

Continuum observing at the CSO began nearly 20 years ago with a single-detector 0.3 K Infrared Labs system which was a respectable effort for that time. Several successful scientific investigations were completed (Lis, Carlstrom, & Keene 1991; Lis & Carlstrom 1994) before the arrival of array detectors, at which point the single bolometer took on a new role as the detector for the Fourier Transform Spectrometer (Serabyn et al. 1998).

The first three submillimeter imaging cameras at CSO were made possible by collaboration with Harvey Moseley's group at NASA/Goddard and also with the SOFIA program and University of Chicago. All used semiconducting bolometers based on doped silicon. A group at Caltech built the SHARC I camera around a monolithic linear 24-element Goddard array (Wang et al. 1995). Meanwhile, a group at U. Chicago made bolometers the old-fashioned way — soldering tiny silicon chips onto tiny thermally-isolating wires — and fielded the Hertz imaging polarimeter with two arrays of 32 detectors each (Schleuning et al. 1997). (Later on, the silicon chips were replaced with NTD germanium for better-controlled resistance; see Dowell et al. 1998.) Work was started at Caltech in the late 1990's on SHARC II, a 384-element 2D array camera which pushes the wiring and power consumption limits of the semiconducting bolometer technology (Dowell et al. 2003). SHARC II was commissioned in late 2002.

The successor to SHARC II at the CSO is likely to be based on a newer detector technology, the microwave kinetic inductance detectors. An initial demon-

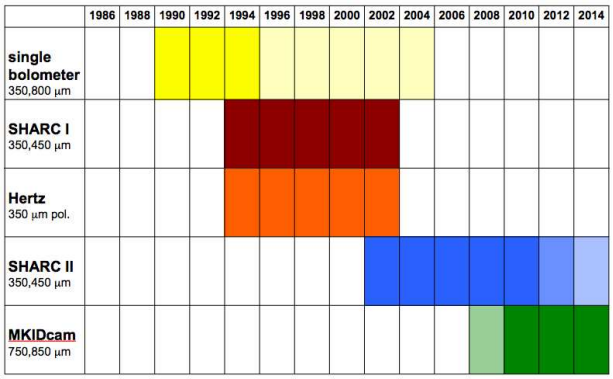

Figure 1. History and future of submillimeter continuum detectors at CSO.

stration of a small MKID array has been made on the way toward a camera with 2304 detectors (Glenn et al. 2008).

2 To Chop or Not To Chop

The single bolometer, SHARC I, and Hertz used traditional chopping mirrors to separate source and atmospheric emission. Signals were recovered by simple on-off subtraction or, for scan mapping, by the NOD2 algorithm (Emerson, Klein, & Haslam 1979). While successful, this approach has the known limitations of poor sensitivity to spatial scales which are near integer multiples of the chop amplitude and of the related ringing around bright sources.

Starting with the Bolocam 1.4/2 mm camera and SHARC II, which have many more detectors covering the telescope field of view, observers have preferred scanning of the telescope without chopping the secondary mirror. SHARC II uses two cross-linked scan patterns described in Figure 2. These choices for observing strategy have led to a few-year educational process about the manner in which 1/f atmospheric noise enters the maps and methods to remove it (e.g., Kovacs 2006; Aguirre et al. 2009).

3 SHARC II Photo Gallery

SHARC II is the submillimeter camera currently in operation at the CSO. I take this opportunity to show some images from the camera that have not yet made their way into publication (Figures 3–5) — two of which depart from astrophysics a bit.

4 Case Study: The Galactic Center

As an example of improvement in continuum mapping speed at the CSO, I show a region toward the Galactic center mapped with the single bolometer system, SHARC I, and SHARC II (Fig. 6). In addition to decreasing the time required to make an observation, improved CSO cameras have also allowed the detection

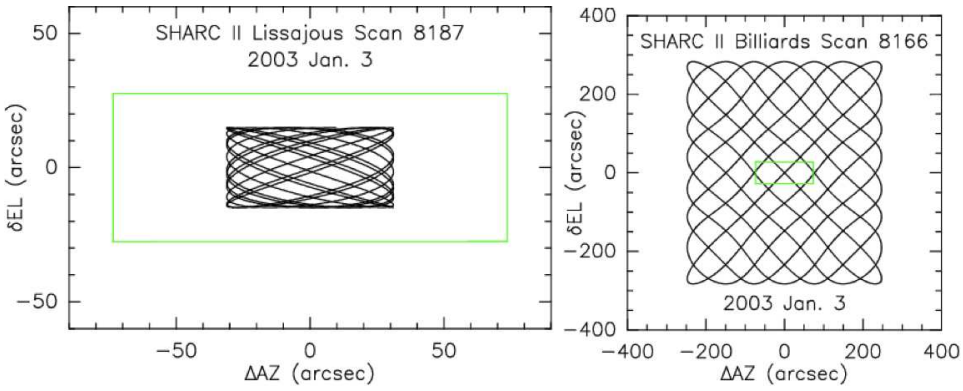

Figure 2. Scan patterns used at the CSO with SHARC II. *Left*: Lissajous pattern used for small fields. The black curve shows the trajectory of the center detector in the array, compared to the green rectangle which shows the size of the full array. Typical periods are 10–20 seconds, and the periods in the two axes are chosen so that the time between pattern repetitions is very long. *Right*: Billiard scan (or 'box scan') pattern used for large fields. In each axis, the motion is a triangle wave vs. time, but with only the first few Fourier terms used in order to smooth the turnarounds. The box shape (not quite square) is chosen to achive good coverage and a pattern period of ∼10 minutes. Both scan patterns achieve good cross-linking.

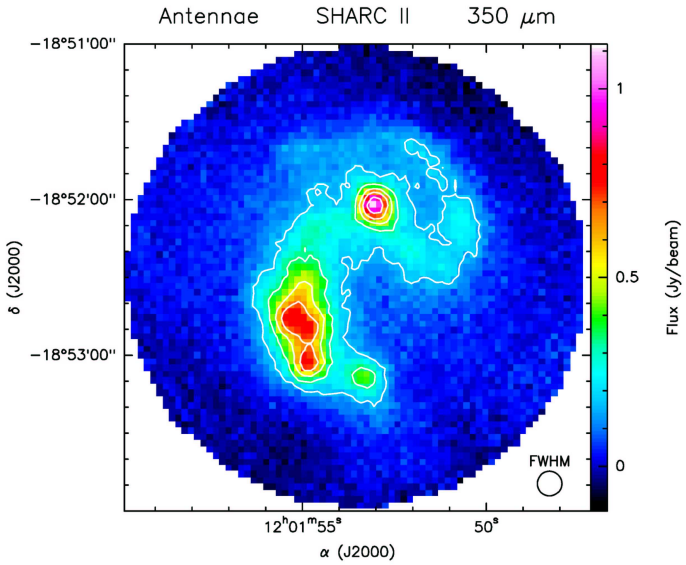

Figure 3. This SHARC II 350 μm image of the Antennae interacting galaxy pair has been referenced as 'private communication' in several reports and proposals, but sadly has not yet found its way into publication. The observations date back to 3 January 2003, and this was the first difficult target attempted with SHARC II. Weather conditions for the 2.3-hour observation were outstanding, and a sensitivity of 8 mJy/beam rms was achieved. Many structures match what is seen in the 15 μm ISO image (Mirabel et al. 1998).

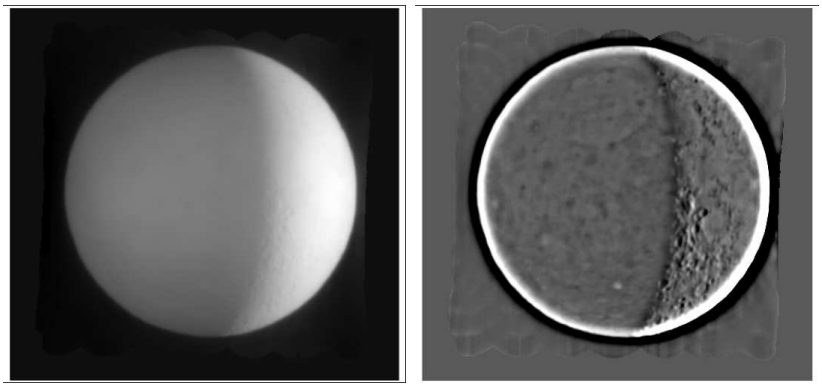

Figure 4. The Moon observed at 850 μm with SHARC II. *Left*: The 'total power' readout and cross-linked scans allow the mapping of large angular scales with low noise. *Right*: The structure at small angular scales shows interesting contrast on the two sides of the terminator in the high-pass filtered image. An interpretation by this amateur solar system astronomer is that the structure to the right of the terminator is dominated by solar-heating-induced variations in temperature, and the structure to the left is dominated by variations in surface emissivity.

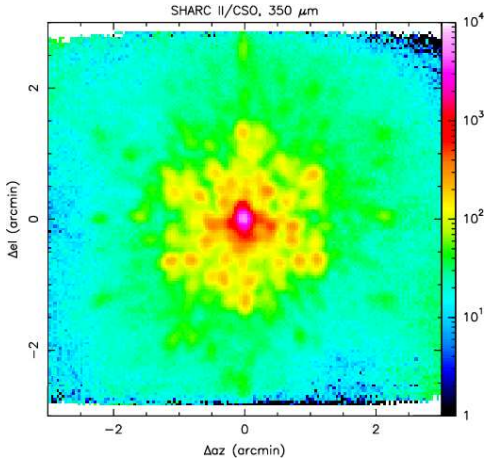

Figure 5. CSO beam structure at 350 μm measured with SHARC II. The source is Mars, and the color scale is logarithmic. SHARC II illuminates the telescope uniformly; the Airy ring which would result with a perfect telescope is only visible at 850 μm, but near sidelobe structure with ∼5% of the main beam power is visible at 350 μm at the approximate location of the Airy ring. The so-called 'error beam' is composed of a multitude of point-like, ∼1%-level maxima in a hexagonal distribution about 2.4 arcminutes across, corresponding to the shape and size of a CSO panel. A lower-level hexagonal pattern with twice the size is also observed.

of Sgr A* (Serabyn et al. 1997), and then the detection of Sgr A* variability (Yusef-Zadeh et al. 2006, 2008), in addition to the mapping of magnetic fields (Chuss et al. 2003).

5 Correlated Photon Noise in SHARC II Array

Since the SHARC II detectors are closely spaced (0.6 λ/D at 350 μm), and the photon mode occupation number is high, adjacent detectors show correlated noise, as can be seen in Figure 7.

Acknowledgments. I thank the following people for supplying material for the conference poster and this paper: Dominic Benford, Ed Bufil, Sunil Golwala, Darek Lis, and John Vaillancourt. Part of the research described in this paper was carried out at the Jet Propulsion Laboratory, California Institute of Technology, under a contract with the National Aeronautics and Space Administration.

References

Aguirre, J., et al. 2009, ApJ, submitted
Bally, J., et al. 2009, in preparation
Chuss, D. T., Davidson, J. A., Dotson, J. L., Dowell, C. D., Hildebrand, R. H., Novak, G., & Vaillancourt, J. E. 2003, ApJ, 599, 1116
Dowell, C. D., Hildebrand, R. H., Schleuning, D. A., Vaillancourt, J. E., Dotson, J. L., Novak, G., Renbarger, T., & Houde, M. 1998, ApJ, 504, 588
Dowell, C. D., Lis, D. C., Serabyn, E., Gardner, M., Kovacs, A., & Yamashita, S. 1999, ASP Conf. Ser., 186, 453
Dowell, C. D., et al. 2003, SPIE, 4855, 73
Emerson, D. T., Klein, U., & Haslam, C. G. T. 1979, A&A, 100, 209
Glenn, J., et al. 2008, SPIE, 7020, 9
Kovacs, A. 2006, Ph. D. thesis, Caltech
Lis, D. C., Carlstrom, J. E., & Keene, J. 1991, ApJ, 380, 429
Lis, D. C., & Carlstrom, J. E. 1994, ApJ, 424, 189
Mirabel, I. F., et al. 1998, A& A, 333, L1
Schleuning, D. A., Dowell, C. D., Hildebrand, R. H., Platt, S. R., & Novak, G. 1997, PASP, 109, 307
Serabyn, E., Carlstrom, J., Lay, O., Lis, D. C., Hunter, T. R., & Lacy, J. H. 1997, ApJ, 490, L77
Serabyn, E., Weisstein, E. W., Lis, D. C., & Pardo, J. R. 1998, Appl. Opt., 37, 2185
Wang, N., et al. 1996, Appl. Opt., 35, 6629
Yusef-Zadeh, F., et al. 2006, ApJ, 644, 198
Yusef-Zadeh, F., Wardle, M., Heinke, C., Dowell, C. D., Roberts, D., Baganoff, F. K., & Cotton, W. 2008, ApJ, 682, 361

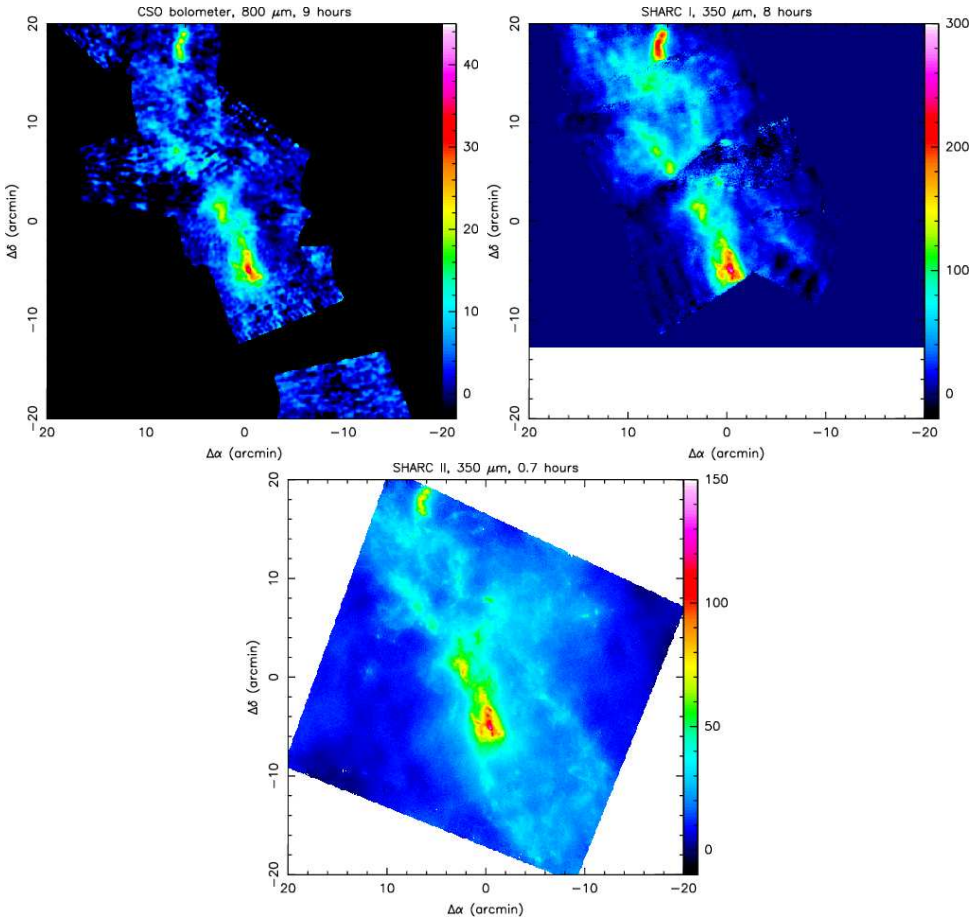

Figure 6. Images of the central half degree of the Galaxy observed with the best available CSO continuum detectors of the early 1990's (*upper left*; Lis & Carlstrom 1994), mid 1990's (*upper right*; Dowell et al. 1999), and mid 2000's (*bottom*; Bally et al. 2009). Although key structures are visible in all three maps, the SHARC II map has clear advantages of better sensitivity per map pixel in a fraction of the observing time, reduced mapping artifacts, and better uniformity of noise — all made possible by the improved mapping speed and observing strategy (a large box scan).

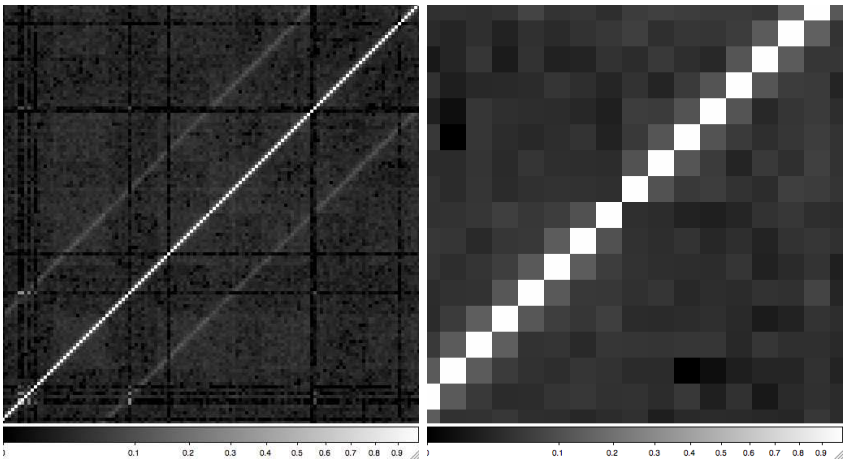

Figure 7. Correlated photon noise in SHARC II signals. The axes in both images follow pixel index, which advances by 32 along a detector row, then advances to the next row. The grayscale indicates the normalized covariance $\left(\sum d_i d_j\right) \left(\sum d_i^2 \sum d_j^2\right)^{-1/2}$, where d_i is the signal from detector i with mean subtracted, and the sum is over time. The *left* panel shows the covariances for approximately 100 detector pairs, emphasizing the significant correlation for detectors separated by an index of 32 — 1 row and 0 columns — leading to the off-diagonal stripes. The typical value of the normalized covariance in these stripes is $\sim$8%. The *right* panel shows the covariances close to the central diagonal; there is another significant correlation of $\sim$8% for detectors separated by an index of 1 — 1 column and 0 rows. (The grayscale values on the central diagonal are 1 by definition.)